Bychkov–Rashba dominated band structure in an $In_{0.75}Ga_{0.25}As–In_{0.75}Al_{0.25}As$ device with spin-split carrier densities of $<10^{11}$ cm^{-2}

2008 J. Phys.: Condens. Matter 20 472207

(http://iopscience.iop.org/0953-8984/20/47/472207)

J. Phys.: Condens. Matter **20** (2008) 472207 (6pp) doi:10.1088/0953-8984/20/47/472207

FAST TRACK COMMUNICATION

Bychkov–Rashba dominated band structure in an $In_{0.75}Ga_{0.25}As$–$In_{0.75}Al_{0.25}As$ device with spin-split carrier densities of $<10^{11}$ cm^{-2}

S N Holmes[1], P J Simmonds[2,3], H E Beere[2], F Sfigakis[2], I Farrer[2], D A Ritchie[2] and M Pepper[1,2]

[1] Toshiba Research Europe Limited, Cambridge Research Laboratory, 208 Cambridge Science Park, Milton Road, Cambridge CB4 0GZ, UK
[2] Cavendish Laboratory, University of Cambridge, J J Thomson Avenue, Cambridge CB3 0HE, UK

E-mail: s.holmes@crl.toshiba.co.uk

Received 19 September 2008
Published 6 November 2008
Online at stacks.iop.org/JPhysCM/20/472207

Abstract
We demonstrate that a Bychkov–Rashba dominated band structure can be stabilized in a nominally undoped $In_{0.75}Ga_{0.25}As$–$In_{0.75}Al_{0.25}As$ quantum well. The transport properties of this system have been measured at 1.7 and 4.2 K and the Rashba coefficient α has been determined in enhancement and depletion modes with an insulated front gate. In enhancement mode, α is 1×10^{-11} eV m with carrier densities n_s between 1.4 and 1.9×10^{11} cm^{-2}. In depletion mode, with $n_s < 1.4 \times 10^{11}$ cm^{-2}, α was reduced to 0.7×10^{-11} eV m. The wavefunction penetration into the $In_{0.75}Al_{0.25}As$ barriers, i.e. the interface asymmetry, makes no contribution to α in this system. We minimize the Zeeman energy spin-splitting in this high g-factor system by analysing only the Shubnikov–de Haas structure below 0.5 T, i.e. for Landau level filling factors >12. The combination of the two spin-split subbands in ρ_{xx} can be separated using a magnetic field modulation technique where analogue $\mathrm{d}\rho_{xx}/\mathrm{d}B$ or $\mathrm{d}^2\rho_{xx}/\mathrm{d}B^2$ signals are measured directly. The $In_{0.75}Ga_{0.25}As$–$In_{0.75}Al_{0.25}As$ quantum well will have applications both in one-dimensional systems and in gate-induced two-dimensional electron gases where a dominant Bychkov–Rashba spin-splitting is required without the complications of an embedded strained InAs well and without a significant contribution from the interface asymmetry at the $In_{0.75}Al_{0.25}As$ barriers.

1. Introduction

Recent one-dimensional split gate channels [1] and quantum point contact devices [2] have made use of narrow band gap $In_{0.75}Ga_{0.25}As$ quantum wells. This is because of the possibilities in high Landé spin g-factor ($|g| = 9$) spintronic devices and the practical demonstration that high mobility material suitable for ballistic transport studies can be grown by MBE with carrier densities (n_s) in the 0.5–3×10^{11} cm^{-2} region [3, 4]. The $In_{0.75}Ga_{0.25}As$ well-$In_{0.75}Al_{0.25}As$ barrier structure provides a system with a large Zeeman energy spin-splitting in moderate magnetic fields and a band structure dominated by the Bychkov–Rashba spin–orbit coupling induced by structural inversion asymmetry (SIA) [5] at zero magnetic field. This potential device technology also relies on insulated gate schemes and recent progress has been made with oxides grown by atomic layer deposition,

[3] Present address: Department of Electrical and Computer Engineering, University of California, Santa Barbara, CA 93106, USA.

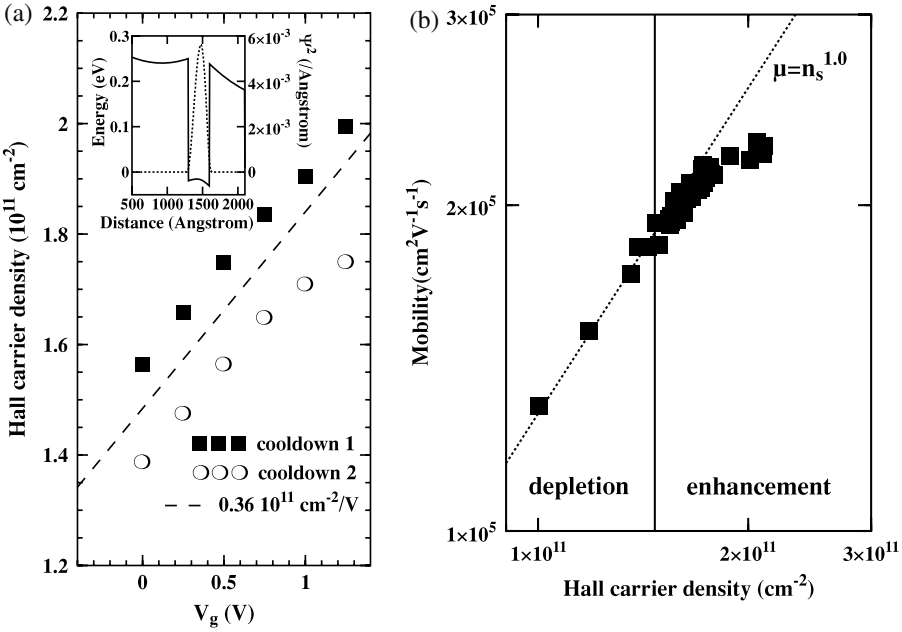

Figure 1. (a) The Hall carrier density as a function of front gate voltage for two different cool downs. The inset shows the self-consistent band structure and wavefunction probability density at $V_g = 0$ V. (b) The dependence of the mobility on Hall carrier density. The accumulated data from seven different cooling cycles is shown.

particularly ZrO_2 [6] and HfO_2 [7] although polyimide resist is used in the present devices. The $In_{0.75}Ga_{0.25}As$–$In_{0.75}Al_{0.25}As$ material system could be used for one-dimensional spintronic devices where the effects of a strong spin–orbit interaction are expected to reveal new physics [8, 9].

Previous measurements of the Bychkov–Rashba coefficient (α) in $In_{0.75}Ga_{0.25}As$ have shown a strong dependence of α on the interface asymmetry contribution compared to the uniform asymmetric electric field across the well [10]. This was achieved with a combination of front and back gating at carrier densities up to 10^{12} cm^{-2}, albeit with an additional 4nm InAs well in the structure. In high carrier density $In_{0.75}Ga_{0.25}As$–$In_{0.75}Al_{0.25}As$ heterostructure devices [11] an α up to 3×10^{-11} eV m was determined and this was attributed to the asymmetry of the wavefunction penetration into the barriers although a Rashba spin-splitting was absent in a 30 nm quantum well structure. In the high magnetic field regime undoped $In_{0.75}Ga_{0.25}As$–$In_{0.75}Al_{0.25}As$ devices have shown a range of many-body effects, such as an enhanced g-factor [12] but no significant Rashba spin-splitting at low magnetic field. An anomalous behaviour [12] in ρ_{xx} at filling factor $\nu = 4$ was attributed to the influence of the Rashba effect.

The present devices are nominally undoped although a background donor state provides approximately 1×10^{11} cm^{-2} electrons in the quantum well. The electrostatics of this background doping contributes to an asymmetric confining potential. This asymmetry in the confining potential and the wavefunction penetration into the barriers has been modelled as a function of carrier density and compared to experimentally determined Bychkov–Rashba coefficients. The modulated magnetic field measurements are sensitive enough that the Bychkov–Rashba spin–orbit coupling effects can be seen up to 4.2 K in a region of magnetic field (<0.5 T) where the Zeeman energy is <10% of the Rashba spin-splitting. This material system could be used as the channel of a spin-FET, or as a spin-polarized current source or have applications to *gate-induced* structures with a large spin–orbit coupling at low carrier density. It will also have uses in devices that reply on g-factor variation in the device but with the added functionality of spin–orbit coupling at zero applied magnetic field.

2. Experimental details

2.1. Device properties

The 30 nm $In_{0.75}Ga_{0.25}As$ quantum well with $In_{0.75}Al_{0.25}As$ barriers was grown in a Veeco Mod Gen II MBE system [4]. Although the device was nominally undoped, a deep level donor in the $In_{0.75}Al_{0.25}As$ barrier was present at a density of $\sim 1 \times 10^{16}$ cm^{-3} [3]. The dark carrier density was 0.4–0.5×10^{11} cm^{-2} at 1.7 K. After saturation illumination with an infrared LED a carrier density in the well of 1.4–1.6 $\times$ 10^{11} cm^{-2} could be stabilized. This could be enhanced or depleted with a polyimide-insulated gate. Hall bar devices defined by optical lithography were measured with and without surface gates for several different cooling cycles to 1.7 K. Figure 1(a) shows the variation in Hall carrier density with front gate voltage (V_g) for two different cool downs in enhancement mode. The measured value of $dn_s/dV_g = 0.36 \times 10^{11}$ cm^{-2} V^{-1}, confirms that the carriers are in the well. There is no parallel conduction in the $In_{0.75}Ga_{0.25}As$ capping layer or the $In_{0.75}Al_{0.25}As$ barriers. In figure 1(b) the mobility (μ) scales as $\mu = n_s^{1.0}$ for $n_s < 2 \times 10^{11}$ cm^{-2}, indicating that it is limited by background impurity scattering. Alloy-disorder scattering dominates at higher carrier densities [13]. The inset to figure 1(a) shows a self-consistent band structure of the

device modelled using a Poisson–Schrödinger solver [14] for $V_g = 0$ V. This is discussed further in section 4.

2.2. Magnetic field modulation

We use a magnetic modulation technique [15] where a time (t) dependant magnetic field ($B_M \cos \omega t$) with frequency ω, and amplitude B_M (between 4.2 and 5.7 mT) is superimposed on the static applied magnetic field (B). The resistance of the device (ρ_{xx} or ρ_{xy}) can be expanded in a Taylor series about the static magnetic field (B) as

$$R(B + B_M \cos \omega t) \approx R(B) + B_M \frac{dR}{dB} \cos \omega t + \frac{1}{4} B_M^2 \frac{d^2R}{dB^2} \cos 2\omega t + O(\cos \omega t)^3 \quad (1)$$

where R represents either ρ_{xx} or ρ_{xy} and $B_M \ll B$. The signals on the device are measured with Stanford SR830 lock-in amplifiers, either at frequency ω or at the second harmonic 2ω, where either dR/dB or d^2R/dB^2 respectively are measured directly. The AC magnetic field was supplied via 1400-turn solenoids of either 36 SWG Cu wire (for temperatures above 10 K) or Cu-clad 18 filament Nb–Ti superconducting wire [16] for temperatures below 10 K. Typical modulation frequencies were 33 Hz with solenoid currents up to 2 A supplied from a battery-powered audio amplifier to minimize 50 Hz mains noise. The modulation field amplitude is constant after a drop of 10% between 0 T and an applied magnetic field of 0.03 T. This is due to the mutual inductance coupling with the static magnetic field solenoid. The dR/dB signal (at frequency ω) also contains the background eddy current signal and induced voltages [15] that complicate the phase of the signal. This can be avoided by measuring d^2R/dB^2 at 2ω where no such background signal is present. The measured two-dimensional electron gas is very homogeneous with different contact geometries showing identical magnetoresistance signals. As expected $d\rho_{xx}/dB$ and $d\rho_{xy}/dB$ are out of phase by $\pi/2$ and ρ_{xx} and $-d^2\rho_{xx}/dB^2$ and have a similar oscillatory structure.

3. Transport measurements

Modulated magnetic field measurements were carried out in applied magnetic fields up to 1 T at either 1.7 or 4.2 K. Three different arrangements of device operation are reported, varying n_s (both in enhancement and depletion modes), varying gate voltage at constant n_s, and an ungated Hall bar geometry. The carrier density regime was always that of single electric subband occupation. The second electric subband is occupied at $n_s > 5 \times 10^{11}$ cm^{-2}. An ungated device shows clear multiple frequencies in $d\rho_{xx}/dB$ and $d^2\rho_{xx}/dB^2$ demonstrating that the effects reported here are not due to edge state reflection at gated–ungated border regions or due to non-uniform gating of n_s. Measuring directly spin-dependent carrier densities is a more sensitive way of quantifying the Bychkov–Rashba coefficient than by analysing the low-field anti-weak localization correction to ρ_{xx} [17]. Magnetoresistance oscillations are seen down to 0.05 T (where $\mu B = 1$) due to the high mobility. In fact the mobility is sufficiently high that a magneto-phonon resonance (MPR) effect is observed in the oscillatory magnetoresistance at 100 K. The MPR fundamental field of 13.0 T agrees reasonably well with the LO-phonon scattering dominated MPR effect in $In_{0.5}Ga_{0.5}As$ where the fundamental field is 12.2 T [18].

3.1. Fast Fourier transform analysis of oscillatory magnetoresistance

The Shubnikov–de Haas effect signals in $d\rho_{xx}/dB$ and $d^2\rho_{xx}/dB^2$ are analysed in the magnetic field domain 0.05–0.5 T. The resolution in the fundamental field (B_f) of the FFT is then 0.05 T. Non-physical features can also be seen in the FFT, such as harmonics and sum and difference frequencies [11]. The double peak structure in the FFTs presented here is due to Rashba spin-splitting and the spin-split carrier densities (n^+, n^-) can be determined from the measured fundamental fields using,

$$n^{\pm} = \frac{e}{h} B_f. \quad (2)$$

The Hall carrier density n_s is then equal to $n^+ + n^-$ and this relationship is observed in both depletion and enhancement modes. The oscillatory signal in $d\rho_{xy}/dB$ can also contain an admixing of $d\rho_{xx}/dB$ due to lithographic mis-alignments and a complicated multiple frequency structure can be observed. In devices presented here a background signal quasi-periodic in B (not $1/B$) can cause extra features in the FFT. This effect can be reduced by changing the field domain to 0.15–0.5 T, although the resolution of the FFT decreases. The non-1/B periodic structure is enhanced at 4.2 K compared with 1.7 K and this can also be seen in a high mobility GaAs–$Al_{0.3}Ga_{0.7}As$ device grown in the same growth sequence. The GaAs–$Al_{0.3}Ga_{0.7}As$ device does not however show multiple frequencies in ρ_{xx} due to a Rashba spin-splitting energy (ΔE_{SIA}) $\approx$ 0.1 meV at an n_s of 10^{11} cm^{-2} [5] as the value of α in GaAs–$Al_{0.3}Ga_{0.7}As$ is 0.069×10^{-11} eV m [19].

3.2. Enhancement mode ($V_g > 0$)

Figure 2 shows $d\rho_{xx}/dB$ up to 0.5 T at 1.7 K as the gate voltage is increased from +0.5 to +1.2 V. A dc current of 200 nA was used to minimize electron heating effects. The device was illuminated at $V_g = 0$ V before incrementing the gate voltage for the set of measurements. The right-hand panel of the figure shows the FFT for each gate voltage in the magnetic field domain 0.15–0.5 T. A clear double peak structure can be seen which is characteristic of Rashba spin-splitting. Opposite magnetic field sweep directions (with different field sweep rates) are shown for comparison in the FFT spectra and reveal good reproducibility.

A second set of data was taken with gate voltages between +0.5 and +1.2 V but illuminating the device after each gate voltage increment. This technique kept the carrier density constant at 1.55×10^{11} cm^{-2} but varied the asymmetry of the confining potential. Although it is difficult to quantify the change in potential by this method, the effect is similar to that of applying a positive backgate voltage [10]. At each gate voltage, $n^+ = 0.69 \times 10^{11}$ cm^{-2} and $n^- = 0.86 \times 10^{11}$ cm^{-2} indicating a constant Bychkov–Rashba coefficient. In all the different gating arrangements, the double peaks in the FFT

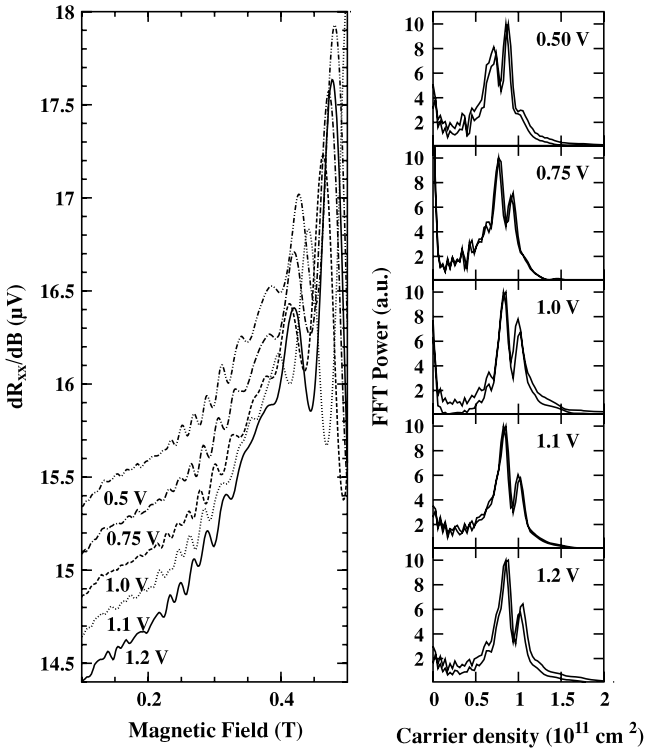

Figure 2. The analogue $\mathrm{d}\rho_{xx}/\mathrm{d}B$ signal up to 0.5 T as a function of front gate voltage at carrier density 1.57, 1.69, 1.83, 1.84 and 1.88×10^{11} cm^{-2}. (The scale of the y-axis is in μV and this corresponds to the analogue signal at 4.4 mT modulation field and 200 nA source–drain current.) The right-hand panel shows the power spectrum at each gate voltage.

spectrum have a similar power showing that the two spin-split subbands have similar quantum mobility. Increasing the field domain for the FFT up to 1 T includes a significant contribution from Zeeman spin-splitting and a single peak in the FFT is then observed with $n^+ = n^-$. In enhancement mode, variations in either carrier density or the asymmetry of the confining potential have little effect on α. This is discussed further in section 4.

3.3. Ungated device

An ungated device was measured to confirm that no contribution to the magneto-oscillations was coming from a non-uniform carrier density in the channel, or due to charge depletion effects in the narrow voltage probes of the device. Three separate cool downs with different cooling rates all yielded similar magnetoresistance signals. Figure 3 shows $\mathrm{d}^2\rho_{xx}/\mathrm{d}B^2$ for an ungated device at 1.7 K up to 0.7 T. This signal size at 2ω is an order of magnitude smaller than that at ω, due partly to the prefactor of the second harmonic in (1).

The double peak structure in the FFT persists up to 4.2 K but the non-$1/B$ periodic magnetoresistance tends to increasingly dominate the FFT spectrum at higher temperatures. This could be related to a magneto-intersubband scattering (MIS) effect between the two spin-split subbands. This non-conventional intersubband scattering might be expected to be seen at magnetic fields below B_{MIS} where

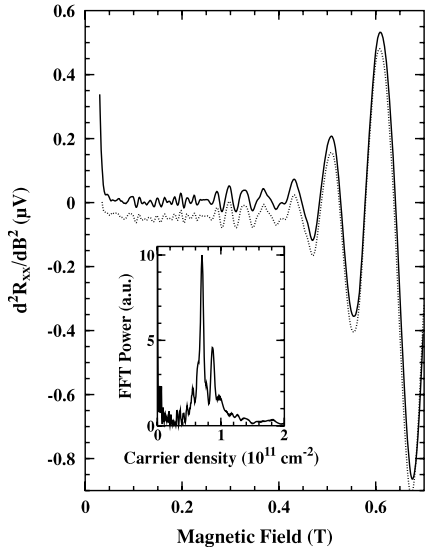

Figure 3. Analogue $\mathrm{d}^2\rho_{xx}/\mathrm{d}B^2$ up to 0.7 T for an ungated device at 1.7 K. Two different sweeps are shown. The y-axis scale is in μV with a modulation field of 5.5 mT and a source–drain current of 100 nA. The inset shows the FFT power spectrum.

$B_{\mathrm{MIS}} = 2\pi m^* \Delta E_{\mathrm{SIA}}/eh$. This corresponds to $B < 0.7$ T with $\Delta E_{\mathrm{SIA}} \approx 2$ meV and $m^* = 0.04m_e$ for $In_{0.75}Ga_{0.25}As$ materials. The more conventional MIS is seen with two electric subbands occupied [20] at carrier densities $>5 \times 10^{11}$ cm^{-2} in the case of a 30 nm wide $In_{0.5}Ga_{0.5}As$ quantum well. The peak(s) in $\mathrm{d}^2\rho_{xx}/\mathrm{d}B^2$ at magnetic fields <0.03 T are partly weak-localization effects and partly experimental artefacts, i.e. due to a change in the modulation field strength (B_{m}), as discussed in section 2.2.

3.4. Depletion mode ($V_g < 0$)

Two sets of measurements in depletion mode at $V_{\mathrm{g}} = -1.0$ and -1.5 V, revealed a reduction in α. At -1.5 V the Hall carrier density is 1.00×10^{11} cm^{-2} and the spin-split carrier densities from the FFT of $\mathrm{d}^2\rho_{xx}/\mathrm{d}B^2$ are $n^+ = 0.46 \times 10^{11}$ cm^{-2} and $n^- = 0.56 \times 10^{11}$ cm^{-2}, showing that in depletion mode $n_s = n^+ + n^-$ to a good approximation.

A separate series of measurements in a ^{3}He system was carried out and ρ_{xx} was measured directly with a 10 nA ac current. At 400 mK in the regime of the quantum Hall effect, there is a spin-splitting in ρ_{xx} at $\nu = 5$ and possibly at $\nu = 7$. However, this corresponds to the dominance of the Zeeman spin-splitting.

4. Modelling of Bychkov–Rashba interaction parameter and comparison with experiment

The confining potential profile has been modelled using a self-consistent Poisson–Schrödinger algorithm [14]. The background n-type doping density in the $In_{0.75}Al_{0.25}As$ is at the 1×10^{16} cm^{-3} level, which provides a carrier density in the well of 1.4×10^{11} cm^{-2} at zero front gate voltage. A thin $In_{0.75}Ga_{0.25}As$ layer at the surface prevents oxidation of $In_{0.75}Al_{0.25}As$ but only has a Schottky barrier of 0.032 eV.

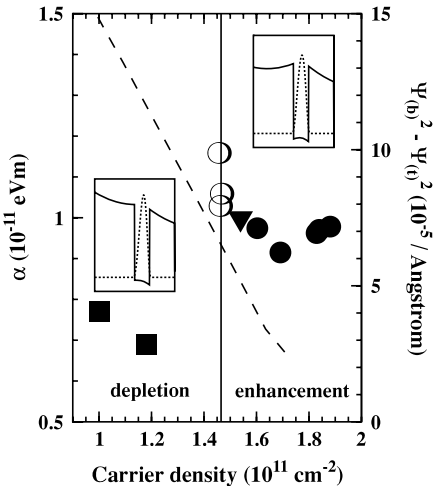

Figure 4. A summary of the experimental Rashba coefficient for different gating measurements including the ungated device. A self-consistent calculation is shown as the dashed line for the normalized wavefunction asymmetry with the scale on the right-hand axis. The symbols represent the following: ■—depletion mode, ○—an ungated device, ▼—enhancement mode with constant n_s and ●—enhancement mode with variable n_s. The asymmetry in the self-consistent band structure is evident in the inset at 1×10^{11} cm^{-2} and at 1.6×10^{11} cm^{-2}.

This gives a small range in enhancement of n_s with a gate, up to a carrier density of 2.0×10^{11} cm^{-2}. With further voltage enhancement, the surface then charges up in the self-consistent model. The effect of the wavefunction asymmetry in the confining potential on the electric field across the well due to the interfaces ($E_{\text{interface}}$) can be quantified using:

$$E_{\text{interface}} = \delta V \frac{1}{e}(|\Psi_{(b)}|^2 - |\Psi_{(t)}|^2) \tag{3}$$

where $\Psi_{(b)}$ and $\Psi_{(t)}$ are the wavefunctions at the bottom and top $In_{0.75}Al_{0.25}As$ interfaces respectively. δV is the conduction band offset between the $In_{0.75}Ga_{0.25}As$ and the $In_{0.75}Al_{0.25}As$. The electric field across the confining potential is additionally dependent on the electrostatics of the doping profile. In depletion mode the asymmetry increases by a factor of 15. This can be seen as the dashed line in figure 4, where the self-consistent value for $|\Psi_{(b)}|^2 - |\Psi_{(t)}|^2$ is calculated as a function of carrier density in the well, as varied by gate voltage. The measured Bychkov–Rashba coefficient should scale with (3) if the asymmetry at the interfaces is providing a contribution to the SIA spin-splitting, as observed at higher carrier density in this material [10, 11].

Experimentally the Bychkov–Rashba coefficients are determined using the difference in spin-split carrier densities assuming a constant density of states, as described in [21]. Non-parabolicity corrections are negligibly small at the carrier densities here. Figure 4 shows a summary of α determined under the different experimental conditions described in this paper. In enhancement mode α is constant at 0.96×10^{-11} eV m, the small variation in α represents a random error of $\pm 0.02 \times 10^{-11}$ eV m. The point ▼ represents the set of data described in section 3.2, taken in enhancement mode but illuminating the device after every gate voltage increase. So although the applied field across the quantum well is changing, the carrier density remains constant. The variation in (nominally identical) data points for the ungated device at constant $n_s = 1.46 \times 10^{11}$ cm^{-2} represents the random experimental error $\pm 0.05 \times 10^{-11}$ eV m in determining α for three different cool downs. The reduction in α in depletion mode, $0.73 \pm 0.04 \times 10^{-11}$ eV m cannot be explained by an interface contribution to the SIA. The insets to figure 4 shows the self-consistent solutions to the Poisson–Schrödinger equation at $n_s = 1 \times 10^{11}$ cm^{-2} (in depletion mode) and $n_s = 1.6 \times 10^{11}$ cm^{-2} (in enhancement mode) where the asymmetry is evident.

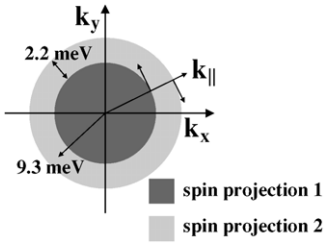

Figure 5. Spin-orientation summary for the $In_{0.75}Ga_{0.25}As$ device and the schematic energy scale at the Fermi surface. The two spin projections are perpendicular to $\mathbf{K}_\parallel$.

The momentum space of the quantum well is shown schematically in figure 5 where the two spin projections, either parallel or anti-parallel to the Rashba effective magnetic field ($\mathbf{B}_R$) are shown. K_x and K_y are the momentum vector components (of $\mathbf{K}_\parallel$) parallel to the plane of the quantum well. The Rashba effective magnetic field is perpendicular to the in-plane momentum, i.e. $\mathbf{B}_R \cdot \mathbf{K}_\parallel = 0$ and this defines the spin-orientation axis for an eigenstate of the confining potential in the presence of spin–orbit coupling. The vector components of $\mathbf{B}_R$ are then given by,

$$\mathbf{B}_R = \frac{1}{\mu_B}\alpha(-k_y, k_x, 0) \tag{4}$$

where μ_B is the Bohr magneton.

The Rashba field $\mathbf{B}_R$ simulates an applied magnetic field only in terms of a spin-splitting energy, however it is much larger than any applied magnetic field here, ~4 T at $|\mathbf{K}_\parallel| = 10^8$ m^{-1}. The spin-splitting energy (ΔE_{SIA}) is given by $2\mu_B|\mathbf{B}_R|$ or $2\alpha|\mathbf{K}_\parallel|$ from (4). The Zeeman energy contribution to the spin-splitting energy is 0.26 meV at 0.5 T and hence can be ignored. In the low carrier density regime investigated here, the $In_{0.75}Ga_{0.25}As$ well system has a ΔE_{SIA} of 2.2 meV compared to a Fermi energy of 9.3 meV (at 1.55×10^{11} cm^{-2}), and the carrier density is $9.2 \pm 0.3\%$ spin-polarized.

5. Conclusions

We have measured the Bychkov–Rashba coefficient in an $In_{0.75}Ga_{0.25}As$ quantum well using a magnetic field modulation technique. This has enabled the Shubnikov–de Haas effect to be quantified in $d\rho_{xx}/dB$ and $d^2\rho_{xx}/dB^2$ at low magnetic fields, without the complications of a Zeeman energy

contribution to the spin-splitting. Despite there being no InAs insert in the middle of the quantum well, we still observe strong spin–orbit coupling due to SIA. The Rashba coefficient is 1×10^{-11} eV m with n_s between 1.4 and 1.9×10^{11} cm^{-2}. In depletion mode with $n_s = 1 \times 10^{11}$ cm^{-2}, α is reduced to 0.7×10^{-11} eV m.

There is no contribution to the spin-splitting from the asymmetry of the wavefunction at the interfaces in the $In_{0.75}Ga_{0.25}As/In_{0.75}Al_{0.25}As$ quantum well system at low n_s, in contrast to previous measurements with a high n_s. This structure will have applications for induced two-dimensional electron gases where a significant Bychkov–Rashba coefficient is present independent of the wavefunction extent at the quantum confinement interfaces. The 1–2 $\times 10^{11}$ cm^{-2} carrier density is the level at which one-dimensional devices will operate and we have demonstrated that in the bulk of the one-dimensional device a Rashba effect is significant and can be quantified.

Acknowledgments

P J Simmonds acknowledges support from the EPSRC. We thank Marc Fletcher for early stage development of insulated gating schemes on this material.

References

[1] Simmonds P J, Sfigakis F, Beere H E, Ritchie D A, Pepper M, Anderson D and Jones G A C 2008 *Appl. Phys. Lett.* **92** 152108
[2] Martin T P, Marlow C A, Samuelson L, Hamilton A R, Linke H and Taylor R P 2008 *Phys. Rev.* B **77** 155309
[3] Capotondi F, Biasiol G, Vobornik I, Sorba L, Giazotto F, Cavallini A and Fraboni B 2004 *J. Vac. Sci. Technol.* B **22** 702
[4] Simmonds P J, Beere H E, Ritchie D A and Holmes S N 2007 *J. Appl. Phys.* **102** 083518
[5] Zawadzki W and Pfeffer P 2004 *Semicond. Sci. Technol.* **19** R1
[6] Koveshnikov S, Goel N, Majhi P, Wen H, Santos M B, Oktyabrsky S, Tokranov V, Kambhampati R, Moore R, Zhu F, Lee J and Tsai W 2008 *Appl. Phys. Lett.* **92** 222904
[7] Lee K Y, Lee Y J, Chang P, Huang M L, Chang Y C, Hong M and Kwo J 2008 *Appl. Phys. Lett.* **92** 252908
[8] Moroz A V and Barnes C H W 1999 *Phys. Rev.* B **60** 14272
[9] Moroz A V and Barnes C H W 2000 *Phys. Rev.* B **61** R2464
[10] Grundler D 2000 *Phys. Rev. Lett.* **84** 6074
[11] Sato Y, Kita T, Gozu S and Yamada S 2001 *J. Appl. Phys.* **89** 8017
[12] Desrat W, Giazotto F, Pellegrini V, Beltram F, Capotondi F, Biasiol G, Sorba L and Maude D K 2004 *Phys. Rev.* B **69** 245324
[13] Capotondi F, Biasiol G, Ercolani D and Sorba L 2005 *J. Cryst. Growth* **278** 538
[14] Snider G 1996 1D Poisson/Schrödinger Band diagram calculator www.nd.edu/∼gsnider
[15] Shoenberg D 1984 *Magnetic Oscillations in Metals* (Cambridge: Cambridge University Press)
[16] Supercon. Inc. Shrewsbury, Massachusetts www.supercon-wire.com
[17] Koga T, Nitta J, Akazaki T and Takayanagi H 2002 *Phys. Rev. Lett.* **89** 046801
[18] Gregoris G, Beerens J, Ben Amor S, Dmowski L, Portal J C, Alexandre F, Sivco D L and Cho A Y 1988 *Phys. Rev.* B **37** 1262
[19] Jusserand B, Richards D, Allan G, Priester C and Etienne B 1995 *Phys. Rev.* B **51** 4707
[20] Simmonds P J, Holmes S N, Beere H E and Ritchie D A 2008 *J. Appl. Phys.* **103** 124506
[21] Engels G, Lange J, Schäpers Th and Lüth H 1997 *Phys. Rev.* B **55** R1958